Supplement of Atmos. Meas. Tech., 17, 4109–4120, 2024
https://doi.org/10.5194/amt-17-4109-2024-supplement

Atmospheric Measurement Techniques
Open Access
EGU

Supplement of

Uncertainties in temperature statistics and fluxes determined by sonic anemometers due to wind-induced vibrations of mounting arms

Zhongming Gao et al.

Correspondence to: Heping Liu (heping.liu@wsu.edu)

Text S1. Investigation of the impact of solar heating on T_s and T_c spectra

To investigate the potential impacts of solar heating on the difference of T_s and T_c spectra, we examined two sets of data, one from nighttime and one from daytime, with similar wind speeds and wind directions (i.e., 7 ms^{-1} < $\bar{u}$ < 9 ms^{-1}; 40 deg < WD < 80 deg). The average normalized power spectra and cospectra were calculated as a function of natural frequency (f) (Figure A1). Both at night (n = 26) and during the day (n = 9), it was observed that the power of T_s spectra was higher in the high frequency range and lower in the low frequency range than T_c. This aligns with the findings in the main text, suggesting that the difference between T_s and T_c spectra was likely not due to solar heating effects on the fine-wire thermocouples. Here n is the number of selected 30-min time series in each group.

Text S2. Investigation of the impacts of wind speed on the spectra distortion in the high frequency range

To investigate the potential causes for the spectral distortion in the high frequency range (i.e., f > 0.2 Hz), we selected two sets of data with similar wind directions but different wind speeds. We then calculated the average normalized power spectra and cospectra as a function of nondimensional frequency ($fz/\bar{u}$, where z is the measurement height, $\bar{u}$ is the mean wind speed; Figure S2). For instance, at the height of 40.2 m, all power spectra of u, w, and T_s illustrated a upturned distortion at the high frequency end (e.g., $fz/\bar{u}$ > 5) due to white noise. Under low wind conditions (i.e., 2 ms^{-1} < $\bar{u}$ < 4 ms^{-1}; 40 deg < WD < 80 deg; n = 126), the power spectra generally followed the –5/3 power law. However, under high wind conditions (i.e., 7 ms^{-1} < $\bar{u}$ < 9 ms^{-1}; 40 deg < WD < 80 deg; n = 70), both the w and T_s spectra were significantly distorted, following a –4/3 power law for approximately 0.5 < $fz/\bar{u}$ < 5. This suggests that the upturned distortion in the T_s spectra was linked to increasing wind speed. For the power spectra for T_c, both groups showed similar declining trends in the high frequency range, indicating that the FW3 was not affected by increased wind speed.

As for the cospectra of w-T_s and w-T_c, they were nearly identical in the high-frequency range (i.e., $fz/\bar{u}$ > 1). This indicates that the above-mentioned distortion in the w, T_s, and T_c spectra had no significant influence on the mean normalized cospectra. Overall, these results suggest that more high-frequency noises/spikes were induced to the time series of T_s with the

increasing wind speeds. While this affected the corresponding spectra somewhat, it had no significant impact on the cospectra. Different tests, where we excluded the first EEMD component with the highest frequency, showed that the spectral distortion in the u, w, and T_s spectra was largely eliminated (dotted lines in Figures S2). This contributed approximately 1–2% to the corresponding variances. Again, the impact on the corresponding cospectra was minor.

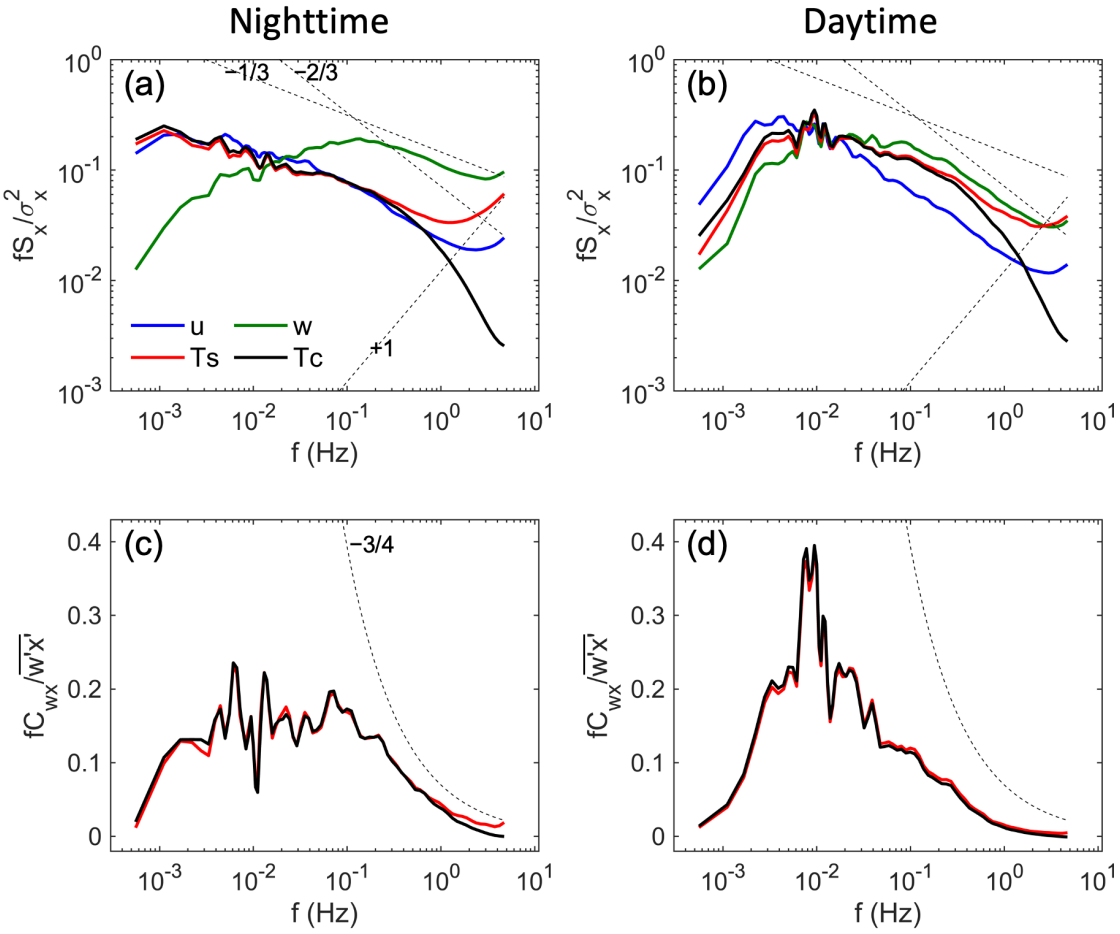

Figure S1. Mean normalized power spectra of u, w, T_s, and T_c and cospectra of the w-T_s and w-T_c for two groups data under the nighttime and daytime conditions with the same wind speed range (7 ms^{-1} < $\bar{u}$ < 9 ms^{-1}) and wind direction range (40 < WD < 80 degree) at the height of 40.2 m. The dashed lines show a $f^{-1/3}$, $f^{-2/3}$, $f^{-3/4}$, and f^{+1} slope.

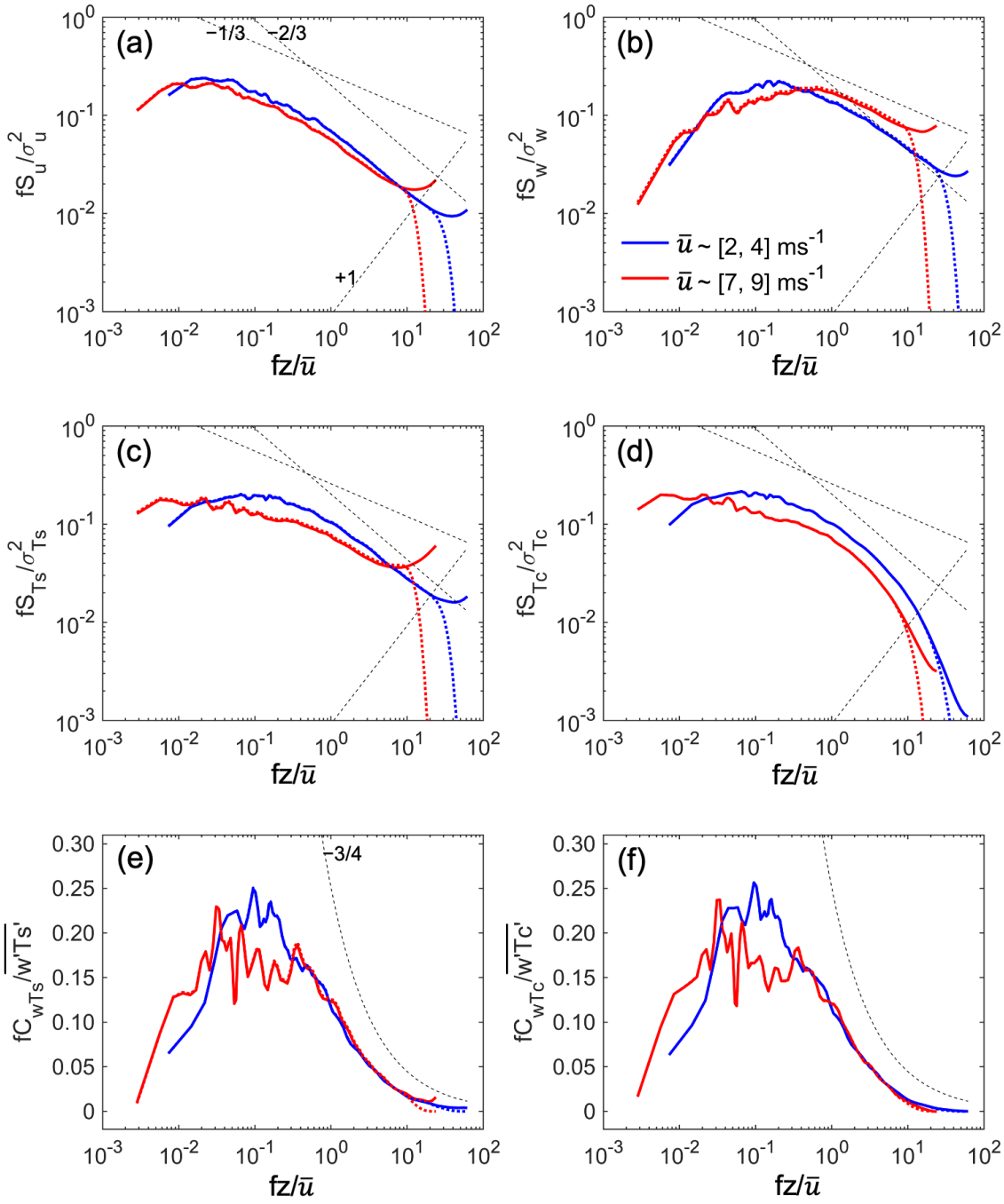

Figure S2. Mean normalized power spectra of u, w, T_s, and T_c and cospectra of the w-T_s and w-T_c for two groups data with different wind speeds but similar wind directions (40 < WD < 80 degree) at the height of 40.2 m. The dotted color lines are the corresponding spectra and cospectra after removing the first EEMD component. The dashed lines show a $f^{-1/3}$, $f^{-2/3}$, $f^{-3/4}$, and f^{+1} slope.

Table S1. Contributions of the three regimes to the total variances and fluxes of water vapor density corrected by T_s and T_c. $\rho'_{v,y}$ refers to the fluctuations of water vapor density corrected by temperature y (i.e., T_s and T_c) using equations (2).

		40.2 m	23.0 m	12.8 m
$\sigma^2_{\rho_{v,Ts},i} / \sigma^2_{\rho_{v,Ts}}$	I	0.76	0.76	0.68
	II	0.18	0.17	0.17
	III	0.06	0.06	0.15
$\sigma^2_{\rho_{v,Tc},i} / \sigma^2_{\rho_{v,Tc}}$	I	0.76	0.77	0.68
	II	0.18	0.17	0.17
	III	0.06	0.06	0.15
$\overline{w'\rho'_{v,Ts}}_i / \overline{w'\rho'_{v,Ts}}$	I	0.64	0.47	0.34
	II	0.31	0.35	0.48
	III	0.04	0.13	0.17
$\overline{w'\rho'_{v,Tc}}_i / \overline{w'\rho'_{v,Tc}}$	I	0.64	0.48	0.35
	II	0.31	0.36	0.48
	III	0.04	0.13	0.16

Table S2. Contributions of the three regimes to the total variances and fluxes of CO_2 concentration corrected by T_s and T_c. $\rho'_{c,y}$ refers to the fluctuations of CO_2 concentration corrected by temperature y (i.e., T_s and T_c) using equations (3).

		40.2 m	23.0 m	12.8 m
$\sigma^2_{\rho_{c,Ts},i} / \sigma^2_{\rho_{c,Ts}}$	I	0.39	0.48	0.26
	II	0.29	0.15	0.23
	III	0.32	0.37	0.51
$\sigma^2_{\rho_{c,Tc},i} / \sigma^2_{\rho_{c,Tc}}$	I	0.40	0.47	0.28
	II	0.31	0.15	0.25
	III	0.29	0.38	0.48
$\overline{w'\rho'_{c,Ts}}_i / \overline{w'\rho'_{c,Ts}}$	I	0.62	0.44	0.09
	II	0.25	0.44	0.26
	III	0.03	0.11	0.57
$\overline{w'\rho'_{c,Tc}}_i / \overline{w'\rho'_{c,Tc}}$	I	0.55	0.37	0.19
	II	0.25	0.40	0.32
	III	0.11	0.20	0.43